# Pharmacological inhibition of temperature-sensitive and Ca$^{2+}$-permeable TRPV3 channel by a natural forsythoside B attenuates pruritus and cytotoxicity of keratinocytes

**Authors:**

Heng Zhang[#], Xiaoying Sun[#], Hang Qi, Qingxia Ma, Qiqi Zhou, Wei Wang and KeWei Wang*

[#]These two authors contributed equally to this paper.

*Correspondence

**Affiliation:**

Department of Pharmacology, School of Pharmacy, Qingdao University, 38 Dengzhou Road, Qingdao 266021, China

JPET # 254045

## Running title page

**Running title:** A novel TRPV3 inhibitor FB reduces pruritus and cytotoxicity

**Corresponding author:** Prof. KeWei Wang

Address: Department of Pharmacology, School of Pharmacy, Qingdao University, 38

Dengzhou Road, Qingdao 266021, China

Tel: 86-532 82991070        E-mail: wangkw@qdu.edu.cn

Number of text pages: 43

Number of figures: 8

Number of references: 46

Words in Abstract: 237

Words in Introduction: 711

Words in Discussion: 709

**Abbreviations**: AEW, acetone-ether-water; CNS, central nervous system; FB,

forsythoside B; FPP, farnesyl pyrophosphate; IPP, isopentenyl pyrophosphate; NFAT,

nuclear factor of activated T-cells; OS, Olmsted Syndrome; RR, ruthenium red; TRP,

transient receptor potential; TRPA1, TRP ankryin 1; TRPV1, TRP vanilloid 1; TRPV3,

TRP vanilloid 3; TRPV4, TRP vanilloid 4; TSLP, thymic stromal lymphopoietin;

2-APB, 2-aminoethoxydiphenyl borate; AITC, allyl isothiocyanate;

JPET # 254045

**Recommended section assignment:**

Behavioral Pharmacology

Cellular and Molecular

Drug Discovery and Translational Medicine

JPET # 254045

## Abstract

Temperature-sensitive and calcium-permeable transient receptor potential vanilloid 3 (TRPV3) channel abundantly expressed in the keratinocyte plays important functions in the skin physiology. Dysfunctional gain-of-function *TRPV3* gene mutations cause genetic Olmsted Syndrome (OS) characterized by periorificial keratoderma, palmoplantar, inflammation and severe itching, suggesting that pharmacological inhibition of overactive TRPV3 function may be beneficial for therapy of pruritus or skin disorders. To test this hypothesis, we identified a natural compound forsythoside B as an inhibitor of TRPV3 through the screen of HEK293 cells expressing human TRPV3 channels in calcium fluorescent assay. Whole-cell patch clamp recordings of HEK293 cells expressing TRPV3 confirmed that forsythoside B selectively inhibited the channel current activated by agonist 2-APB (50 µM) in dose-dependent fashion with an $IC_{50}$ value of $6.7 \pm 0.7$ µM. *In vivo* evaluation of scratching behavior demonstrated that pharmacological inhibition of TRPV3 by forsythoside B significantly attenuated acute itch induced by either TRPV3 agonist carvacrol or pruritogen histamine, and also chronic itch induced by acetone-ether-water in mouse model of dry skin. Furthermore, forsythoside B was able to prevent cell death of HEK293 cells or native HaCaT cells from human keratinocytes expressing gain-of-function TRPV3 G573S mutant or in the presence of TRPV3 agonist carvacrol. Taken together, our findings demonstrate the crucial role of TRPV3 in pruritus and keratinocyte toxicity, thus specific inhibition of overactive TRPV3 by

JPET # 254045

natural forsythoside B may possess therapeutic potential for chronic pruritus, skin

allergy or inflammation-related skin diseases.

JPET # 254045

## Introduction

The warm temperature-activated and calcium-permeable nonselective cation transient receptor potential vanilloid 3 (TRPV3) channel is most abundantly expressed in the skin keratinocytes, and plays a crucial role in numerous physiological processes such as cutaneous sensation, hair growth and skin barrier formation (Cheng et al., 2010; Aijima et al., 2015). The dysfunctional TRPV3 channel function caused by genetic gain-of-function mutations or pharmacological activation is implicated in the pathogenesis of skin inflammation, dermatitis and chronic itch (Asakawa et al., 2006; Imura et al., 2009; Lin et al., 2012; Cui et al., 2018). In rodents, a spontaneous gain-of-function mutation of *TRPV3* gene in WBN/Kob-Ht rats (Gly573 substituted by Cys) and DS-*Nh* mice (Gly573 substituted by Ser) causes the development of skin lesions with pruritus and dermatitis (Asakawa et al., 2006; Imura et al., 2009; Yoshioka et al., 2009; Yamamoto-Kasai et al., 2013), and silencing of TRPV3 attenuates itch sensation or inflammatory pain (Bang et al., 2012; Yamamoto-Kasai et al., 2012; Sun et al., 2018). We have previously reported three gain-of-functional mutations of TRPV3 (W692G, G573C and G573S) from Chinese patients with genetic Olmsted Syndrome (OS) featured by mutilating palmoplantar keratoderma with dermatitis, periorificial keratotic plaguesand severe itching (Lin et al., 2012). Inside-out or whole-cell patch clamp recordings demonstrate that these TRPV3 mutants are constitutively open with robust inward currents (Xiao et al., 2008; Lin et al., 2012) and elevation of intracellular $Ca^{2+}$ that subsequently triggers cell death of keratinocytes (Lin et al., 2012). The similar gain-of-function TRPV3 mutations were

also reported from other counties in OS patients characterized by dermatitis and severe itching (Duchatelet et al., 2014; Eytan et al., 2014; Kariminejad et al., 2014; Choi et al., 2018). All these observations demonstrate that TRPV3 channel emerges as a promising therapeutic target, and specific inhibition of overactive TRPV3 may present therapeutic potential for treatment of chronic pruritus or skin diseases that are unmet medical needs.

As a polymodal sensor, the ligand-gated TRPV3 is also activated by a number of chemicals including 2-aminoethoxydiphenyl borate (2-APB), intracellular proton, endogenous ligand farnesyl pyrophosphate (FPP) and natural compounds including carvacrol, thymol and camphor (Chung et al., 2004; Xu et al., 2006; Bang et al., 2010; Cao et al., 2012; Cui et al., 2018). TRPV3 is also inhibited by 2-APB structural analog DPTHF (Chung et al., 2005), isopentenyl pyrophosphate (IPP) (Bang et al., 2011), 17(R)-resolvin D1 (anti-inflammatory lipid mediator) (Bang et al., 2012), TRPM8 and TRPA1 channel agonist icilin (Sherkheli et al., 2012), $Mg^{2+}$ (Luo et al., 2012) and TRP channel broad-spectrum inhibitor ruthenium red (Nilius et al., 2007). However, there is lack of selective TRPV3 antagonists, which hampers the pharmacological studies of TRPV3 channel function. Thus, it is imperative to discover specific TRPV3 inhibitors that can be used to validate TRPV3 as a therapeutic target and to treat skin diseases associated with overactive TRPV3 function.

*Lamiophlomis rotate,* also known as Tibetan Duyiwei and grown in Tibet and Southwestern areas of China, is commonly used as a traditional Chinese herbal

medicine to alleviate detumescence, inflammation and pain (Jiang et al., 2010a; Zhu et al., 2014). As an active ingredient of the leaves of *L. rotata,* forsythoside B (FB) is a phenylethanoid glycoside suppressing inflammatory responses via inhibiting NF-κB signaling (Jiang et al., 2010a; Jiang et al., 2010b; Jiang et al., 2012). A recent observation also demonstrates that activation of TRPV3 induces inflammatory response mediated by NF-κB signaling (Szollosi et al., 2018). Based on these investigations, we hypothesized that forsythoside B might act as an inhibitor of TRPV3.

In this study, we utilized a calcium influx fluorescent assay and found that natural compound forsythoside B is able to specifically inhibit TRPV3 channel activity in a dose-dependent fashion. *In vivo* evaluation demonstrates that forsythoside B exerts anti-pruritic effects on acute itch induced by TRPV3 agonist carvacrol or pruritogen histamine, and chronic itch induced by acetone-ether-water in mouse model of dry skin. Forsythoside B also prevents cell death triggered by TRPV3 gain-of-function mutation or agonist carvacrol in either HEK293 cells expressing TRPV3 channels or native HaCaT cells from human skin keratinocyte cell line. Our findings demonstrate that specific inhibition of TRPV3 by natural compound forsythoside B attenuates pruritus and cell death of keratinocytes, suggesting a therapeutic potential of forsythoside B for chronic pruritus, dermatitis or skin-inflammation related diseases.

## Materials and Methods

### Reagents and compounds

Natural compound forsythoside B (FB) with molecular mass at 756.7 g/mol and purity over 99% was obtained from Taoto Biotech Corporation, Ltd. (Shanghai, China). The chemical structure of forsythoside B is shown as Figure 1. TRPV3 agonists 2-aminoethoxydiphenyl borate (2-APB) and carvacrol, TRPV1 agonist capsaicin, TRPA1 agonist allyl isothiocyanate (AITC), TRPV4 agonist GSK1016790A (GSK101) and TRP channel antagonist ruthenium red (RR) were obtained from Sigma-Aldrich Corporation (St. Louis, MO, USA). Reports of HPLC analyses of these standard compounds indicate their compound purity of no less than 98.0%. With the exception of RR dissolved in water, stock solutions of forsythoside B (100 mM), GSK101 (500 μM) and 2-APB (1 M) were prepared in dimethyl sulfoxide (DMSO). The final DMSO concentration in each compound solution was not exceeding 0.2%. The stock solution of capsaicin in 100 mM was prepared in absolute ethanol. Compounds used for the measurement of intracellular fluorescent calcium were diluted in the Hanks' balanced salt solution (HBSS). For whole-cell patch clamp recordings, all compounds were prepared in perfusion solution. With the exception of carvacrol dissolved in 10% ethanol, the compounds used in evaluation of scratching behaviors were diluted in normal saline.

### Animals

C57BL/6 male mice at age of 6-8 weeks were purchased from the Vital River Laboratory Animal Technology Co., Ltd. (Beijing, China). Evaluation of pruritic

scratching behavior was carried out after their acclimatization at their housing environment for at least 7 days. Mice were housed and maintained in the environment with a 12-h light/12-h dark cycle and the controlled temperature of 22.0 ± 2.0 °C. Mouse food and water were *ad libitum* accessible to mice. All experimental protocols for animals were approved by the Institutional Animal Care and Use Committee of Qingdao University. All *in vivo* experiments were carried out in compliance with national and institutional guidelines for the care and use of laboratory animals.

**Cell culture**

The human embryonic kidney cell (HEK293) and human immortalized nontumorigenic keratinocyte (HaCaT) cells were cultured in the Dulbecco's minimal essential medium with supplement of 10% of fetal bovine serum (FBS) at 37 °C with % ?? and 5% $CO_2$. HEK293 cells were seeded in a 12-well plate for intracellular calcium measurement. For whole-cell patch clamp recordings, HEK293 cells were cultured on glass coverslips. HEK293 cells were transiently transfected with individual cDNA plasmids of hTRPV3, hTRPV1, hTRPV4, and hTRPA1 using Lipofectamine 2000 (Invitrogen). For identification of transfected cells, all plasmids were tagged with GFP for whole-cell patch clamp recordings. Human TRPV3 plasmids including wild type or mutant G573S were described previously (Lin et al., 2012), and correct TRPV3 mutation was verified by DNA sequencing.

**Measurement of intracellular fluorescent calcium in FlexStation 3 assay**

The Cal-520$^{TM}$ PBX Calcium Assay Kit (AAT Bioquest, Sunnyvale, CA) was used to detect the change of intracellular calcium ($[Ca^{2+}]_i$) in a population of cells

10

using Multi-Mode Microplate Reader in FlexStation 3 assay (Molecular Devices, San Jose, CA). HEK293 cells were transfected with cDNAs of TRP channels before seeded at a density of ~40,000 cells per well in a 96-well black-walled plate (Thermo Fisher Scientific, Waltham, MA) for an overnight culture at 37 °C with 5% $CO_2$. For measurement of intracellular calcium, cells were incubated with the calcium fluorescent dye provided in the Cal-520$^{TM}$ PBX Calcium Assay Kit at 37 °C for 1.5 h, and the values of relative fluorescence unit (RFU) were measured in FlexStation3 under the excitation wavelength at 485 nm and emission wavelength at 515 nm at an interval of 1.6 s (Sun et al., 2018).

**Electrophysiology**

Whole-cell patch clamp recordings were carried out using an EPC10 amplifier driven by PatchMaster software (HEKA, Instrument Inc). The borosilicate glass pipette was pulled using a DMZ-Universal puller (Zeitz-Instruments, GmbH), and was fire polished to a resistance of 3-4 MΩ. Both bath solution and pipette solution used for whole-cell recordings contained (in mM) 130 NaCl, 3 HEPES and 0.2 EDTA, with pH adjusted at 7.2 (Wei et al., 2016). TRP channel current was recorded in cells held at 0 mV in response to a voltage ramp from -100 mV to +100 mV for 500 ms, and the current was analyzed at ± 80 mV. The Origin 8.6 software (OriginLab, Northampton, MA) was used to analyze the data.

**Evaluation of pruritic scratching behavior**

For assessment of itch scratching behavior, the hair of mouse right neck in rostral part was shaved 24 h before the start of experiments using electric hair clipper. The

scratching behavior was recorded on videos. The number of itch scratching bouts was counted through video playback analysis. One scratching bout was counted when a mouse raised right hindlimb to the injection site and continuously scratched for any time length before the limb returned to mouth or floor (Wilson et al., 2013). All behavioral experiments were conducted in a double blind manner (Sun et al., 2018).

For test of acute itch induced by TRPV3 agonist carvacrol or pruritogen histamine, a mouse was put in an observation box with the size of $9 \times 9 \times 13$ cm$^3$ for acclimatization for about 30 min. Carvacrol (0.1%) or histamine (100 μM) in 50 μl was intradermally injected into the right neck. To access the effect of forsythoside B on itch scratching, vehicle (0.3% DMSO) or forsythoside B (3, 30 and 300 μM) was intradermally injected 30 min prior to intradermal injection of agonist carvacrol. For video recordings of acute itch induced by histamine, vehicle (0.03% DMSO) or forsythoside B (0.3, 3, 30 μM) was intradermally injected 30 min prior to intradermal injection of 100 μM pruritogen histamine (Cui et al., 2018; Sun et al., 2018).

For acetone-ether-water (AEW)-induced dry skin of chronic itch, the bare skin of mouse right nape was smeared with acetone and ether (1:1) mixture or water for 15 s, followed by water treatment for 30 s for a period of 5 days (Miyamoto et al., 2002; Yamamoto-Kasai et al., 2012). On the day 6, a mouse was placed in an observation box with the size of 9 cm × 9 cm × 13 cm for acclimatization about 30 min. Different concentrations of forsythoside B (0.3, 3, 30 μM) or vehicle of 0.03% DMSO were intradermally injected into mouse right nape in 50 μl of total volume, and the

scratching was recorded on video for 60 min following the intradermal injection of forsythoside B.

For the test of locomotor activity, a mouse was observed in an open-field chamber with built-in infrared photo sensors after the intradermal injection of forsythoside B in 50 μl (0.3, 3, 30 and 300 μM) into the right neck. Locomotor activity as total distance traveled in the open-field chamber was analyzed for 60 min.

**Cell death assay**

HEK293 cells or HaCaT cells of human skin cell line were seeded in 6-well plate and randomly divided into different groups. After administration of compounds for 12 h, cell death was determined by Hoechst 33258 dye (Thermo Fisher Scientific, USA) labeling for all cell nuclei, and propidium iodide (PI) dye (Thermo Fisher Scientific, USA) labeling for the nuclei of dead cells. In each group, five images were randomly taken under microscopy (Nikon Eclipse Ti, Tokyo, Japan) and automatically counted on a confocal microscopy (Nikon A1R MP, Tokyo, Japan). Cell death ratio was represented by the average of PI labeled cells over Hoechst labeled cells from five images. Because the transfection ratio for WT TRPV3 or G573S TRPV3 mutant was maintained low at about $22.47\% \pm 1.56$ at 12 h in HEK293 cells, cell death ratio was normalized in mutant G573S-induced cell death in HEK293 cells.

**Statistical analysis**

All data are expressed as the means ± S.E.M. Student's *t* test (two-tailed, unpaired) or one-way ANOVA by GraphPad Prism 7.0 software was utilized to analyze the statistical significance (*$p<0.05$, **$p<0.01$, ***$p<0.001$, ****$p<0.0001$). An $IC_{50}$

value was determined by the half of maximal inhibitory concentration of tested compounds.

**Molecular docking**

Docking calculations were completed using the AutoDock 4.2 program (Morris et al., 1998). The 3D structure of forsythoside B was generated by the PRODRG2 sever (Schuttelkopf and van Aalten, 2004). AutoDockTools were used to convert the structure of forsythoside B into AutoDock 4.2 format for docking to the structure of TRPV3 channel protein (PDB code: 6DVW) (Singh et al., 2018). As TRPV3 is composed of 4 identical subunits, one subunit was used to dock forsythoside B compound. For each atom of the macromolecules, Gasteiger charges were calculated and an electrostatic map and a desolvation map were computed by AutoDock 4.2. The Lamarckian genetic algorithm (LGA) was used in the docking simulation for ligand conformational searching according to the standard protocol. All figures of structural models were generated by PyMOL (https://pymol.org/).

## Results

### Identification of natural compound forsythoside B as a TRPV3 inhibitor

We started screening for inhibitory effect of compounds on increase of intracellular calcium caused by activating hTRPV3 channels transiently expressed in HEK293 cells in calcium fluorescent assay using FlexStation3 multi-mode microplate reader. Each compound was added onto a well of 96-well black-walled plate at 17 sec prior to addition of TRPV3 agonist 2-APB at 100 s. The RFU values were measured for another 80 s. Adding of forsythoside B reduced the intracellular $Ca^{2+}$ influx caused by 200 μM 2-APB in HEK293 cells expressing hTRPV3 channels (Fig. 2A). Increasing forsythoside B concentrations (50 μM, 100 μM and 200 μM) dose-dependently reduced the intracellular $Ca^{2+}$ influx mediated by activation of TRPV3 channels, as compared with 50 μM ruthenium red (RR), a broad-spectrum TRP channel blocker.

To confirm the inhibition of TRPV3 current by forsythoside B, we carried out whole-cell patch clamp recordings of HEK293 cells expressing TRPV3 channels. Perfusion of 50 μM forsythoside B significantly reduced the channel current elicited by 50 μM 2-APB about $81.5 \pm 6.8$ % (Fig. 2B). Increasing different concentrations (1 μM to 100 μM) of forsythoside B caused a dose-dependent inhibition of TRPV3 channel current with an $IC_{50}$ value of $6.7 \pm 0.7$ μM (Fig. 2C). These results indicate that forsythoside B inhibits TRPV3-mediated $Ca^{2+}$ influx or TRPV3 current induced by agonist 2-APB.

### Selective inhibition of TRPV3 channel current by forsythoside B

To determine the selectivity of forsythoside B, we examined the effects of

JPET # 254045

forsythoside B on other thermoTRP channels such as TRPV1, TRPV4 and TRPA1 channels that have previously been reported to be involved in itch signaling (Zhang, 2015; Chen et al., 2016). The channel currents were activated by a voltage ramp from -100 mV to +100 mV for 500 ms. Perfusion of forsythoside B (50 µM) only had a slight reduction about $12.1 \pm 3.7$ % of TRPV1 current induced by 1 µM selective agonist capsaicin (Fig. 3, A and D) or about $14.8 \pm 4.9$ % of TRPV4 current induced by 50 nM selective agonist GSK101 (Fig. 3, B and D), or about $10.9 \pm 4.5$ % of TRPA1 channel current evoked by 300 µM AITC (Fig. 3, C and D), as compared with 81.5% inhibition of TRPV3 current by forsythoside B (50 µM). These data indicate the selective inhibition of TRPV3 by natural compound forsythoside B over other thermoTRPs such as TRPV1, TRPV4 and TRPA1 channels.

**Forsythoside B suppresses acute itch induced by pruritogen carvacrol or histamine**

Our recent observations show that pharmacological activation of TRPV3 channel by carvacrol can evoke scratching behavior in mice (Cui et al., 2018). To determine the inhibitory effect of forsythoside B on TRPV3 activation-induced itch, we made an intradermal injection of forsythoside B into mouse neck 30 min before the injection of carvacrol into the same site. After intradermal injection of carvacrol (0.1%), the spontaneous scratching bouts were dramatically increased about 5.7-fold to $188.9 \pm 35.5$ (n=9, ***$p < 0.001$) from $33 \pm 4.1$ (n=7) for the group of vehicle (10% ethanol)within 30 min (Fig. 4A). In contrast, intradermal injection of 30 µM or 300 µM forsythoside B led to a dramatic decrease of scratching bouts to $83.7 \pm 23.8$ (n=9,

16

*p<0.05) and 45.6 ± 6.4 (n=7, **p<0.01), respectively (Fig. 4A). These results indicate that forsythoside B suppresses the scratching behavior induced by TRPV3 agonist carvacrol.

Histamine, the most common pruritogen, causes acute itch in human or rodents (Sun and Dong, 2016). The histamine level in the skin from DS-*Nh* mice carrying gain-of-function TRPV3 mutation is substantially higher as compared to age-matched DS mice (Asakawa et al., 2006). Similarly, TRPV3 knockout mice also exhibit attenuation of pruritus evoked by histamine (Sun et al., 2018). Thus, we further tested the effect forsythoside B on histamine-dependent acute itch evoked by histamine. As shown in Figure 4B, intradermal injection of 100 μM histamine into mouse nape led to a dramatic increase in spontaneous scratching behavior with the number of bouts at 52.2 ± 6.4 within 30 min (n=6, **p< 0.01) as compared to vehicle control at 3.4 ± 1.8 (n=5). Pretreatments with different concentrations (0.3, 3 or 30 μM) of forsythoside B significantly reduced the scratching bouts in a dose-dependent manner to 22.5 ± 7.7 (n=6, **p<0.01), 15.5 ± 4.9 (n=6, ***p<0.001) and 5.8 ± 1.6 (n=6, ***p<0.001), respectively (Fig. 4B), indicating that forsythoside B suppresses histamine-induced scratching behavior.

**Forsythoside B attenuates pruritic scratching behavior in mouse model of dry skin**

Investigations from others and ours show that dry skin induced by AEW evokes spontaneous scratching in normal mice but not TRPV3 knockout mice (Miyamoto et al., 2002; Yamamoto-Kasai et al., 2012; Sun et al., 2018). We therefore further tested

the effect of TRPV3 inhibition by forsythoside B on scratching behavior in model of dry skin induced by AEW treatment. The mouse skin of nape becomes dry with white dandruff after five-day treatment of AEW as compared with vehicle control of water treatment (Sun et al., 2018). On the day 6, different concentrations of forsythoside B (0.3, 3, 30 μM in 50 μl) or vehicle of DMSO (0.03%) were intradermally injected into the right nape after acclimatization for 30 min. The itch scratching behavior was recorded on video for 60 min following the intradermal injections. As shown in Figure 4C, AEW treatment induced a significant increase in spontaneous scratching bouts with a number of $39.8 \pm 6.4$ (n=5, **$p<0.01$), as compared with the blank control of water treatment at $8.1 \pm 2.5$ (n=7) within 60 min. In contrast, application of 3 μM and 30 μM forsythoside B significantly reduced itch scratching bouts to $15.1 \pm 4.6$ (n=8, *$p<0.05$) and $9.8 \pm 4.0$ (n=9, **$p<0.01$), respectively.

To exclude any possible sedative effects caused by forsythoside B, locomotor activity assessment was performed following the intradermal injection of different concentrations of forsythoside B into the nape of mouse neck within 60 min. As shown in figure 4D, administration of different concentrations of forsythoside B (0.3-300 μM in 50 μl) had no significant alteration in the total distance traveled in the chambers. These results suggest that forsythoside B attenuates dry skin-induced chronic itch likely through direct inhibition of TRPV3 channel function.

**Forsythoside B attenuates cell death in HEK293 or HaCaT cells expressing constitutively open TRPV3 G573S mutant in a dose-dependent manner**

We have previously observed that keratinocytes from keratotic lesions of OS

18

patient skin undergo significant apoptosis with higher cell death ratio (Lin et al., 2012), indicating that the cell death of keratinocytes is characteristic of dermatitis or skin diseases. Co-transfection of WT TRPV3 with the gain-of-function G573S mutant in HEK293 cells has been shown to partially rescue the cell death triggered by the G573S mutant (Xiao et al., 2008), suggesting that inhibition of TRPV3 can protect cell death from overactive TRPV3 function. We determined the cell death ratio by PI staining for dead cells over Hoechst staining of all cells. As shown in, The normalized cell death ratio was maintained at low level of 6.78 ± 2.04% in HEK293 cells transfected with WT TRPV3 (Figure 5A and B), indicating that transfecting WT TRPV3 had little effect on triggering cell death. In contrast, transfection of TRPV3 G573S mutant significantly increased the cell death ratio to 48.61 ± 6.45%. Incubation of 10 μM and 100 μM forsythoside B effectively reduced the cell death ratio to 26.76 ± 4.97% and 16.78 ± 3.97%, respectively, as compared with non-specific TRPV3 inhibitor ruthenium red (20 μM) that had little rescue effect on cell death (Figure 5A and B).

Since forsythoside B was able to reduce the cytotoxicity of cells heterologously expressing the gain-of-function TRPV3 mutant, we further tested whether forsythoside B had any protective effect on HaCaT cells originated from human keratinocytes. As shown in Figure 5C and D, HaCaT cells transfected with G573S mutant for 12 h significantly increased cell death ratio compared to normal HaCaT cells (n=4, ****$p<0.0001$). Adding non-specific TRPV3 inhibitor RR at 20 μM had no rescue effect on cell death. In contrast, 100 μM forsythoside B partially reduced

cell death (*$p$<0.05). Our results indicate that inhibition of TRPV3 by forsythoside B can attenuate cell death induced by overactive TRPV3 in both HEK293 cells and human HaCaT cells.

**Forsythoside B reduces cytotoxicity induced by carvacrol in both HEK293 cells expressing TRPV3 and HaCaT cells**

Atopic dermatitis is featured of cell death in the keratinocytes, and pharmacological activation of TRPV3 by its agonist monoterpenoid carvacrol also can induce cell death in normal human epidermal keratinocytes (NHEK) cells (Szollosi et al., 2018). To further confirm the specific inhibition of TRPV3 by forsythoside B, we tested the inhibitory effect of forsythoside B on TRPV3 current activated by 300 μM carvacrol in HEK293 cells expressing TRPV3. As shown in Figure 6A and B, forsythoside B can dose-dependently inhibited TRPV3 current. We also further tested the rescue effect of forsythoside B on cell death in HEK293 cells expressing WT TRPV3 and human HaCaT cells. In HEK293 cells expressing WT TRPV3, 300 μM carvacrol treatment for 12 h caused significant cell death of 23.3 ± 2.59% (Figure 6C and D). Incubation of 10 μM and 100 μM forsythoside B effectively reduced the cell death ratio to 12.83 ± 1.48% and 11.66 ± 1.32%, respectively. As compared with forsythoside B, RR also had a partial rescue effect on cell death. Interestingly, 300 μM carvacrol was unable to induce cell death in normal HEK293 cells, suggesting carvacrol-induced cytotoxicity is dependent on the presence of TRPV3.

Similarly, HaCaT cells treated with 300 μM carvacrol for 12 h significantly increased the cell death ratio (Fig. 6E and F). Treatment of HaCaT cells with

20

forsythoside B caused reduction of cell death, consistent with the results obtained from HEK293 cells (Figure 6D). Our results indicate that pharmacological inhibition of TRPV3 by forsythoside B can reduce cytotoxicity triggered by agonist in cells expressing TRPV3 channels.

**Putative binding sites by docking of forsythoside B into the cryo-EM structure of mouse TRPV3**

The cryo-electron microscopy structure of a full-length mouse TRPV3 both in closed apo and agonist-bound open state was recently solved at 4.3 Å (Singh et al., 2018). Based on the structure, we attempted to explore where and how compound forsythoside B binds to and causes the inhibition of TRPV3 channel function. To identify the potential TRPV3 binding sites for forsythoside B, we utilized AutoDock 4.2 program to dock forsythoside B into the mouse TRPV3 structure (Figure 7A and B). Our docking results show a putative binding pocket for forsythoside B that is formed by residues T636 from the pore helix and F666 from S6 of one subunit and G638 and L639 from the selectivity filter of the neighboring subunit (Figure 7C). As a result, forsythoside B inhibits the channel activity of TRPV3 by binding to the region between the selectivity filter and the central cavity of TRPV3 (Figure 7D), thus likely making ions impermeable for passing through the intracellular gate of TRPV3 (Singh et al., 2018). Nevertheless, this binding site needs to be further validated by site-directed mutagenesis.

## Discussion

In this study, our purpose was to identify a specific TRPV3 inhibitor as tool that can be utilized to validate TRPV3 as a therapeutic target for treatment of chronic pruritus and dermatitis-related skin diseases. Using the calcium fluorescent assay in multi-plate reader format, we screened and identified a natural compound forsythoside B that attenuates itch scratching behavior, and reduces cell death caused by overactive TRPV3. Our findings demonstrate that specific inhibition of TRPV3 by natural forsythoside B may present a promising therapy for chronic pruritus and skin inflammation related diseases.

Accumulating evidence suggests that the warm temperature-sensitive and calcium permeable TRPV3 channel plays a pivotal role in itch sensation, skin physiology and pathology (Wang and Wang, 2017), although other Thermo-TRP channels have been reported to be involved in itch signaling (Zhang, 2015). The most convincing evidence for TRPV3 as a novel target for pruritus comes from the observations on spontaneous mutations of TRPV3 that cause dermatitis in rodents, and on human genetic gain-of-function mutations in Olmsted Syndrome (OS) patients characterized by atopic dermatitis and intolerable itchiness (Imura et al., 2009; Yoshioka et al., 2009; Lin et al., 2012; Duchatelet et al., 2014; Eytan et al., 2014; Kariminejad et al., 2014; Choi et al., 2018). Silencing of TRPV3 reduces itch scratching behavior in mice (Yamamoto-Kasai et al., 2012). Conversely, pharmacological activation of TRPV3 by natural pruritogen carvacrol induces scratching, whereas carvacrol-mediated itching is

significantly attenuated in TRPV3 knockout mice (Cui et al., 2018). Those lines of accumulated evidence indicate the critical role of TRPV3 in pruritus.

Natural compound forsythoside B is also an active ingredient of the fruit of *Forsythia suspensa*, which exhibits potent pharmacological activities of antipyretic and anti-inflammation (Muluye et al., 2014). Extracts from *F. suspensa* can suppress the release of inflammatory mediators such as nitric oxide (NO) and pro‑inflammatory cytokines prostaglandin E2 (PGE2), and also reduce the level of inflammatory factors TNF-α and IL-6 (Lee et al., 2010; Lee et al., 2011). Forsythoside B also decreases endothelin-1 (ET-1, another pruritogen) secretion, cyclooxygenase-2 (COX-2) activity, and inhibits NF-κB signaling to exert its anti-inflammatory effects (Sahpaz et al., 2002; Martin-Nizard et al., 2004; Jiang et al., 2010a). In this study, our findings reveal a previously unknown mechanism of action for forsythoside B that inhibits TRPV3 channel, which may help explain its broad anti-inflammatory effects. Forsythoside B can also be used as a tool for further validating TRPV3 as a therapeutic target for skin diseases such as atopic dermatitis or chronic pruritus.

In this study, we proposed a mechanism underlying the causative role of overactive TRPV3 in itch sensation and cytotoxicity of keratinocytes. Overactive TRPV3 induced by gain-of-function of G573S mutation or pharmacological activation by pruritogen carvacrol causes an excessive influx of calcium in the keratinocytes (Figure 8). Calcium influx activates calcineurin that dephosphorylates the nuclear factor of activated T-cells (NFAT) and induces NFAT translocation from the cytosol to the nucleus for promotion of the transcription and secretion of thymic

JPET # 254045

stromal lymphopoietin (TSLP) (Wilson et al., 2013; Yamamoto-Kasai et al., 2013). The activation of TRPV3 also causes the release of histamine in the skin (Asakawa et al., 2006). The released TSLP, histamine and cytokines from keratinocytes stimulate afferent nerve endings which transmit the itch signal to the central nerve system (CNS) via dorsal horn of spinal cord, thus evoking scratching behavior (Wilson et al., 2013; Bautista et al., 2014). For overactive TRPV3-mediated cytotoxicity, the calcium overload results in cell death of keratinocytes and keratinization or skin diseases via activation of unidentified $Ca^{2+}$-dependent kinase (Figure 8) (Xiao et al., 2008; Cao et al., 2012; Lin et al., 2012). Pharmacological inhibition of TRPV3 by forysthoside B that likely binds to the region between the selectivity filter and the central cavity attenuates itch signaling and cytotoxicity. However, the detailed mechanisms of how TRPV3 activation induces the increase of histamine and how excessive influx of calcium triggers cell death remain to be further investigated.

In summary, we identified a novel TRPV3 inhibitor natural forsythoside B that attenuates both acute and chronic itch by inhibition of TRPV3 channel function. Forsythoside B reduces cytotoxicity caused by either gain-of-function TRPV3 mutation or channel agonist carvacrol. Therefore, the natural compound forsythoside B may be beneficial for treatment of pruritus and keratinocyte toxicity-related skin inflammation and diseases.

JPET # 254045

## Acknowledgements

## Authorship Contributions

Participated in research design: Heng Zhang, Xiaoying Sun, KeWei Wang

Conducted experiments: Heng Zhang, Xiaoying Sun, Hang Qi, Qingxia Ma

Contributed new reagents or analytic tools: Qiqi Zhou, Wei Wang

Performed data analysis: Heng Zhang, Xiaoying Sun

Wrote or contributed to the writing of the manuscript: Heng Zhang, Xiaoying Sun, KeWei Wang

JPET # 254045

# References

Aijima R, Wang B, Takao T, Mihara H, Kashio M, Ohsaki Y, Zhang JQ, Mizuno A, Suzuki M, Yamashita Y, Masuko S, Goto M, Tominaga M and Kido MA (2015) The thermosensitive TRPV3 channel contributes to rapid wound healing in oral epithelia. *FASEB J* **29**:182-192.

Asakawa M, Yoshioka T, Matsutani T, Hikita I, Suzuki M, Oshima I, Tsukahara K, Arimura A, Horikawa T, Hirasawa T and Sakata T (2006) Association of a mutation in TRPV3 with defective hair growth in rodents. *J Invest Dermatol* **126**:2664-2672.

Bang S, Yoo S, Yang TJ, Cho H and Hwang SW (2010) Farnesyl pyrophosphate is a novel pain-producing molecule via specific activation of TRPV3. *J Biol Chem* **285**:19362-19371.

Bang S, Yoo S, Yang TJ, Cho H and Hwang SW (2011) Isopentenyl pyrophosphate is a novel antinociceptive substance that inhibits TRPV3 and TRPA1 ion channels. *Pain* **152**:1156-1164.

Bang S, Yoo S, Yang TJ, Cho H and Hwang SW (2012) 17(R)-resolvin D1 specifically inhibits transient receptor potential ion channel vanilloid 3 leading to peripheral antinociception. *Br J Pharmacol* **165**:683-692.

Bautista DM, Wilson SR and Hoon MA (2014) Why we scratch an itch: the molecules, cells and circuits of itch. *Nat Neurosci* **17**:175-182.

Cao X, Yang F, Zheng J and Wang K (2012) Intracellular proton-mediated activation of TRPV3 channels accounts for the exfoliation effect of alpha-hydroxyl acids on keratinocytes. *J Biol Chem* **287**:25905-25916.

Chen Y, Fang Q, Wang Z, Zhang JY, MacLeod AS, Hall RP and Liedtke WB (2016) Transient receptor potential vanilloid 4 ion channel functions as a pruriceptor in epidermal keratinocytes to evoke histaminergic itch. *J Biol Chem* **291**:10252-10262.

Cheng X, Jin J, Hu L, Shen D, Dong XP, Samie MA, Knoff J, Eisinger B, Liu ML, Huang SM, Caterina MJ, Dempsey P, Michael LE, Dlugosz AA, Andrews NC, Clapham DE and Xu H (2010) TRP channel regulates EGFR signaling in hair morphogenesis and skin barrier formation. *Cell* **141**:331-343.

Choi JY, Kim SE, Lee SE and Kim SC (2018) Olmsted Syndrome Caused by a Heterozygous p.Gly568Val Missense Mutation in TRPV3 Gene. *Yonsei Med J* **59**:341-344.

Chung MK, Guler AD and Caterina MJ (2005) Biphasic currents evoked by chemical or thermal activation of the heat-gated ion channel, TRPV3. *J Biol Chem* **280**:15928-15941.

Chung MK, Lee H, Mizuno A, Suzuki M and Caterina MJ (2004) 2-aminoethoxydiphenyl borate activates and sensitizes the heat-gated ion channel TRPV3. *J Neurosci* **24**:5177-5182.

Cui TT, Wang GX, Wei NN and Wang K (2018) A pivotal role for the activation of TRPV3 channel in itch sensations induced by the natural skin sensitizer carvacrol. *Acta Pharmacol Sin* **39**:331-335.

Duchatelet S, Pruvost S, de Veer S, Fraitag S, Nitschke P, Bole-Feysot C, Bodemer C and Hovnanian A (2014) A new TRPV3 missense mutation in a patient with Olmsted syndrome and erythromelalgia. *JAMA Dermatol* **150**:303-306.

Eytan O, Fuchs-Telem D, Mevorach B, Indelman M, Bergman R, Sarig O, Goldberg I, Adir N and Sprecher E (2014) Olmsted syndrome caused by a homozygous recessive mutation in TRPV3. *J Invest Dermatol* **134**:1752-1754.

Imura K, Yoshioka T, Hirasawa T and Sakata T (2009) Role of TRPV3 in immune response to development of dermatitis. *J Inflamm (Lond)* **6**:17.

JPET # 254045

Jiang WL, Fu FH, Xu BM, Tian JW, Zhu HB and Jian H (2010a) Cardioprotection with forsythoside B in rat myocardial ischemia-reperfusion injury: relation to inflammation response. *Phytomedicine* **17**:635-639.

Jiang WL, Tian JW, Fu FH, Zhu HB and Hou J (2010b) Neuroprotective efficacy and therapeutic window of Forsythoside B: in a rat model of cerebral ischemia and reperfusion injury. *Eur J Pharmacol* **640**:75-81.

Jiang WL, Yong X, Zhang SP, Zhu HB and Jian H (2012) Forsythoside B protects against experimental sepsis by modulating inflammatory factors. *Phytother Res* **26**:981-987.

Kariminejad A, Barzegar M, Abdollahimajd F, Pramanik R and McGrath JA (2014) Olmsted syndrome in an Iranian boy with a new de novo mutation in TRPV3. *Clin Exp Dermatol* **39**:492-495.

Lee JY, Cho BJ, Park TW, Park BE, Kim SJ, Sim SS and Kim CJ (2010) Dibenzylbutyrolactone lignans from *Forsythia koreana* fruits attenuate lipopolysaccharide-induced inducible nitric oxide synthetase and cyclooxygenase-2 expressions through activation of nuclear factor-kappab and mitogen-activated protein kinase in RAW264.7 cells. *Biol Pharm Bull* **33**:1847-1853.

Lee S, Shin S, Kim H, Han S, Kim K, Kwon J, Kwak JH, Lee CK, Ha NJ, Yim D and Kim K (2011) Anti-inflammatory function of arctiin by inhibiting COX-2 expression via NF-kappaB pathways. *J Inflamm (Lond)* **8**:16.

Lin Z, Chen Q, Lee M, Cao X, Zhang J, Ma D, Chen L, Hu X, Wang H, Wang X, Zhang P, Liu X, Guan L, Tang Y, Yang H, Tu P, Bu D, Zhu X, Wang K, Li R and Yang Y (2012) Exome sequencing reveals mutations in TRPV3 as a cause of Olmsted syndrome. *Am J Hum Genet* **90**:558-564.

Luo J, Stewart R, Berdeaux R and Hu H (2012) Tonic inhibition of TRPV3 by $Mg^{2+}$ in mouse epidermal keratinocytes. *J Invest Dermatol* **132**:2158-2165.

Martin-Nizard F, Sahpaz S, Kandoussi A, Carpentier M, Fruchart JC, Duriez P and Bailleul F (2004) Natural phenylpropanoids inhibit lipoprotein-induced endothelin-1 secretion by endothelial cells. *J Pharm Pharmacol* **56**:1607-1611.

Miyamoto T, Nojima H, Shinkado T, Nakahashi T and Kuraishi Y (2002) Itch-associated response induced by experimental dry skin in mice. *Jpn J Pharmacol* **88**:285-292.

Morris GM, Goodsell DS, Halliday RS, Huey R, Hart WE, Belew RK and Olson AJ (1998) Automated docking using a Lamarckian genetic algorithm and an empirical binding free energy function. *J Comput Chem* **19**:1639-1662.

Muluye RA, Bian Y and Alemu PN (2014) Anti-inflammatory and antimicrobial effects of heat-clearing Chinese herbs: a current review. *J Tradit Complement Med* **4**:93-98.

Nilius B, Owsianik G, Voets T and Peters JA (2007) Transient receptor potential cation channels in disease. *Physiol Rev* **87**:165-217.

Sahpaz S, Garbacki N, Tits M and Bailleul F (2002) Isolation and pharmacological activity of phenylpropanoid esters from *Marrubium vulgare*. *J Ethnopharmacol* **79**:389-392.

Schuttelkopf AW and van Aalten DM (2004) PRODRG: a tool for high-throughput crystallography of protein-ligand complexes. *Acta Crystallogr D Biol Crystallogr* **60**:1355-1363.

Sherkheli MA, Gisselmann G and Hatt H (2012) Supercooling agent icilin blocks a warmth-sensing ion channel TRPV3. *The Scientific World J* **2012**:982725.

Singh AK, McGoldrick LL and Sobolevsky AI (2018) Structure and gating mechanism of the transient receptor potential channel TRPV3. *Nat Struct Mol Biol* **25**:805-813.

Sun S and Dong X (2016) Trp channels and itch. *Semin Immunopathol* **38**:293-307.

Sun XY, Sun LL, Qi H, Gao Q, Wang GX, Wei NN and Wang K (2018) Antipruritic effect of natural coumarin osthole through selective inhibition of thermosensitive TRPV3 channel in the skin. *Mol Pharmacol* **94**:1164-1173.

Szollosi AG, Vasas N, Angyal A, Kistamas K, Nanasi PP, Mihaly J, Beke G, Herczeg-Lisztes E, Szegedi A, Kawada N, Yanagida T, Mori T, Kemeny L and Biro T (2018) Activation of TRPV3 regulates inflammatory actions of human epidermal keratinocytes. *J Invest Dermatol* **138**:365-374.

Wang G and Wang K (2017) The $Ca^{2+}$-permeable cation transient receptor potential TRPV3 channel: an emerging pivotal target for itch and skin diseases. *Mol Pharmacol* **92**:193-200.

Wei NN, Lv HN, Wu Y, Yang SL, Sun XY, Lai R, Jiang Y and Wang K (2016) Selective activation of nociceptor TRPV1 channel and reversal of inflammatory pain in mice by a novel coumarin derivative Muralatin L from *Murraya alata*. *J Biol Chem* **291**:640-651.

Wilson SR, The L, Batia LM, Beattie K, Katibah GE, McClain SP, Pellegrino M, Estandian DM and Bautista DM (2013) The epithelial cell-derived atopic dermatitis cytokine TSLP activates neurons to induce itch. *Cell* **155**:285-295.

Xiao R, Tian J, Tang J and Zhu MX (2008) The TRPV3 mutation associated with the hairless phenotype in rodents is constitutively active. *Cell Calcium* **43**:334-343.

Xu H, Delling M, Jun JC and Clapham DE (2006) Oregano, thyme and clove-derived flavors and skin sensitizers activate specific TRP channels. *Nat Neurosci* **9**:628-635.

Yamamoto-Kasai E, Imura K, Yasui K, Shichijou M, Oshima I, Hirasawa T, Sakata T and Yoshioka T (2012) TRPV3 as a therapeutic target for itch. *J Invest Dermatol* **132**:2109-2112.

Yamamoto-Kasai E, Yasui K, Shichijo M, Sakata T and Yoshioka T (2013) Impact of TRPV3 on the development of allergic dermatitis as a dendritic cell modulator. *Exp Dermatol* **22**:820-824.

Yoshioka T, Imura K, Asakawa M, Suzuki M, Oshima I, Hirasawa T, Sakata T, Horikawa T and Arimura A (2009) Impact of the Gly573Ser substitution in TRPV3 on the development of allergic and pruritic dermatitis in mice. *J Invest Dermatol* **129**:714-722.

Zhang X (2015) Targeting TRP ion channels for itch relief. *Naunyn Schmiedebergs Arch Pharmacol* **388**:389-399.

Zhu B, Gong N, Fan H, Peng CS, Ding XJ, Jiang Y and Wang YX (2014) Lamiophlomis rotata, an orally available Tibetan herbal painkiller, specifically reduces pain hypersensitivity states through the activation of spinal glucagon-like peptide-1 receptors. *Anesthesiology* **121**:835-851.

**Footnotes**

JPET # 254045

**Figure legends**

**Figure 1. Chemical structure of natural compound forsythoside B.**

**Figure 2. Identification of natural forsythoside B as an inhibitor for hTRPV3 channels expressed in HEK-293 cells**. **A**, Dose-dependent inhibition of intracellular $Ca^{2+}$ increase mediated through activation of TRPV3 channels in response to 200 μM 2-APB by different concentrations of forsythoside B ranging from 50 μM to 200 μM in FlexStation3 calcium fluorescent assay. In the right panel, a summary for inhibition of intracellular fluorescent $Ca^{2+}$ increase from the left panel. RR: ruthenium red; Blank control: 0.2% DMSO; FB: forsythoside B. Asterisks denote statistical significance compared with RR control (n=6, *$p$<0.05, by one-way ANOVA). **B,** Whole-cell patch clamp recordings of TRPV3 currents in response to 2-APB alone (50 μM, red bar) or co-application of 50 μM forsythoside B (FB, blue bar). In the right panel**,** current-voltage curves of hTRPV3 in response to voltage ramps from -100 mV to + 100 mV before (1), and after 50 μM 2-APB (2), and co-addition of 50 μM 2-APB and 50 μM forsythoside B (3) and washout (4). **C,** Left panel, representative hTRPV3 currents in response to 50 μM 2-APB before and after its co-addition with increasing concentrations of forsythoside B (from 1 μM to 100 μM). Right panel, curve fitting of dose-dependent inhibition of 2-APB-mediated hTRPV3 activation by forsythoside B with an $IC_{50}$ of 6.7 ± 0.7 μM (n=5~10). Data are presented as the means ± S.E.M.

30

**Figure 3. Selective inhibition of TRPV3 current by forsythoside B over TRPV1, TRPV4 and TRPA1 channels. A,** Representative hTRPV1 current activated by 1 μM capsaicin (red bar) before and after its co-application with 50 μM forsythoside B (FB, blue bar) and washout. Right panel: Current-voltage curves of hTRPV1 in response to voltage ramps from -100 mV to + 100 mV from the left panel before (1) and after 1 μM capsaicin (2), after co-addition of 50 μM forsythoside B and 1 μM capsaicin (3), and washout (4). **B,** Representative hTRPV4 current activated by 50 nM GSK101 (red bar) or in the absence or presence of 50 μM forsythoside B (FB, blue bar) before inhibition by 20 μM ruthenium red (RR, pink bar); right panel: Current-voltage curves of hTRPV4 in response to voltage ramps from -100 mV to + 100 mV from the left panel before (1) and after 50 nM GSK101 (2), co-addition of 50 μM forsythoside B and 50 nM GSK101 (3), and 20 μM RR (4). **C,** Representative hTRPA1 current activated by 300 μM allyl isothiocyanate (AITC, red bar) or in the absence or presence of 50 μM forsythoside B (FB, blue bar) before complete inhibition by 20 μM ruthenium red (RR, pink bar); right panel: current-voltage curves of hTRPA1 in response to voltage ramps from -100 mV to + 100 mV from the left panel before (1) and after 300 μM AITC (2), co-addition of 50 μM forsythoside B and 300 μM AITC (3), and 20 μM RR (4). **D,** Summary for percentage inhibition of hTRPV3, hTRPV1, hTRPV4 and hTRPA1 channel activation by 50 μM forsythoside B. Data are presented as the means ± S.E.M. Asterisks denote statistical significance as compared with hTRPV3 control (n=5~6, ***$p<0.001$, by unpaired $t$-test).

**Figure 4. Forsythoside B reduces scratching behavior induced by carvacrol and histamine or AEW in mice**. **A,** Left panel, the time course of neck-scratching activity was observed in C57BL/6 mice after intradermal injection carvacrol (0.1%) in 50 μl into mouse neck, with pretreatment of vehicle (0.3% DMSO) and different concentrations (3, 30, 300 μM) of forsythoside B in 50 μl in the same site. Time for scratching bouts was plotted for each 5 min bin over 30 min. Right panel, quantification of scratching bouts during 30 min of left panel (n=7~9, N.S., no significance, $*p<0.05$, $**p<0.01$, $***p<0.001$, by one-way ANOVA). **B,** Left panel, representative the time course of neck-scratching activity was observed after intradermal injection histamine (100 μM) 50 μl into mouse neck, with pretreatment of vehicle (0.03% DMSO) and different concentrations (0.3, 3, 30 μM) of forsythoside B in 50 μl into the same site. Time for scratching bouts was plotted for each 5 min bin over 30 min. Right panel, quantification of scratching bouts during 30 min of left panel (n=5~6, N.S., no significance, $**p<0.01$, $***p<0.001$, by one-way ANOVA). **C,** Dose-dependent inhibition of spontaneous scratching bouts in AEW-treated mice by pretreating with topical application of forsythoside B (n=5~9, N.S., no significance, $*p<0.05$, $**p<0.01$, by one-way ANOVA). **D,** Locomotor activity assessment (total travel distance, cm) after intradermal injection with forsythoside B (0.3, 3, 30, 300 μM, 50 μl/site) into the nape of the mouse neck (n=5, N.S., no significance, by one-way ANOVA).

**Figure 5. Forsythoside B reduces cell death of HEK 293 cells and HaCaT cells expressing the gain-of-function TRPV3 G573S mutant.** A, Forsythoside B reduced

the death of HEK293 cells expressing TRPV3 G573S mutant in a dose-dependent manner. Representative Hoechst staining of cell nuclei (top images) and propidium iodide (PI) staining for dead cells (bottom images). Scale bar = 100 μm. B, The statistical analysis for normalized cell death from panel A. Five independent experiments were performed. Data are presented as the means ± S.E.M. C, Forsythoside B reduced the death of HaCaT cells expressing TRPV3 G573S mutant in a dose-dependent manner. D, Summary of bar graph for panel C, and four independent experiments were performed. Data are presented as the means ± S.E.M.

**Figure 6. Forsythoside B attenuates cell death in HEK293 expressing TRPV3 channels or HaCaT cells activated by TRPV3 agonist carvacrol. A,** Left panel, representative hTRPV3 current in response to 300 μM carvacrol (red bar) before and after its co-addition with RR (pink bar). Right panel, representative hTRPV3 current activated by 300 μM carvacrol (red bar) in the absence or presence of forsythoside B from 1 μM to 100 μM (FB, blue bar) and washout. **B,** A summary of TRPV3 current in response to different compounds of panel A (n=6, by one-way ANOVA). **C,** Cell death assay after transient transfection with WT TRPV3 and following different compounds treatment for 12 h in HEK 293 cells. Scale bar = 100 μm. **D,** Summary for cell death ratio after treatment of different compounds (n=4). **E,** Cell death assay after different compound treatment for 12 h in HaCaT cells. Scale bar = 100 μm. **F,** Summary for cell death ratio after treatment of different compounds (n=4). Data are presented as the means ± S.E.M. *$p < 0.05$, **$p < 0.01$, ***$p < 0.001$, ****$p < 0.0001$.

**Figure 7. Putative binding pocket for forsythoside B bound to the central cavity of mouse TRPV3. A,** Representative view of coronal section for forsythoside B bound to the structure of TRPV3 subunits labeled in different colors of green, pink, purple and cyan for each subunit. Four forsythoside B molecules bound to the binding pocket are also labeled in different colors of red, blue, purple and hotpink. **B,** Top view of four forsythoside B molecules bound to TRPV3 structure. **C,** Expanded view of putative binding sites of forsythoside B in TRPV3. Different subunits of TRPV3 are shown in different colors, and forsythoside B is shown in yellow mesh. The surrounding residues T636 from the pore helix and F666 from S6 of one subunit in green and G638 and L639 from the selectivity filter of the neighboring subunit in yellow are shown as blue sticks and indicated by white arrows. **D,** Schematic diagram illustrating inhibition of TRPV3 by forsythoside B based on the model proposed by Singh et al (Singh et al., 2018). Left panel, putative lipids (blue) are located between the S1-S4 (orange) and S5-S6 (blue) domains in the closed state. Middle panel, open TRPV3 upon binding of agonist 2-APB (in green triangles) to the top of S1-S4 domains, and bringing the S1-S4 and pore domains close together. Forsythoside B (in red) binds to the putative pocket formed by residues from S6 and pore helices of TRPV3, thus blocking the region right below the selectivity filter and the central cavity (right panel).

**Figure 8. Proposed mechanism for the causative role of overactive TRPV3 in itch signaling and cytotoxicity of keratinocytes.** For TRPV3-mediated itch signaling,

activation of TRPV3 by channel agonist carvacrol or gain-of-function mutation results in an elevation of intracellular calcium that leads to activation of calcineurin. The calcineurin dephosphorylates nuclear factor of activated T cells (NFAT) and induces the translocation of NFAT from cytosol to the nucleus. Translocation of NFAT induces transcription of thymic stromal lymphopoitin (TSLP), and thus promotes the secretion of TSLP in the keratinocytes. Released TSLP, histamine and cytokines by TRPV3 activation stimulate the afferent nerve endings that transmit the itch signal through dorsal horn of spinal cord to the CNS to evoke scratching behavior. For overactive TRPV3-mediated cytotoxicity, the excessive influx of calcium induces the cell death of keratinocytes via activation of unidentified $Ca^{2+}$-dependent kinase.
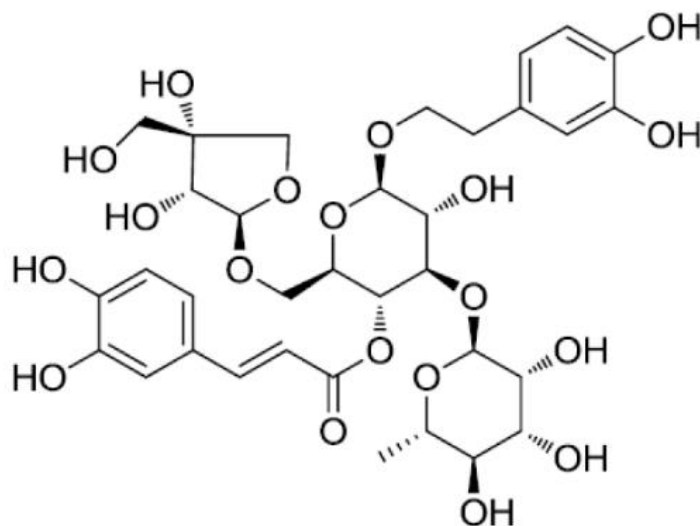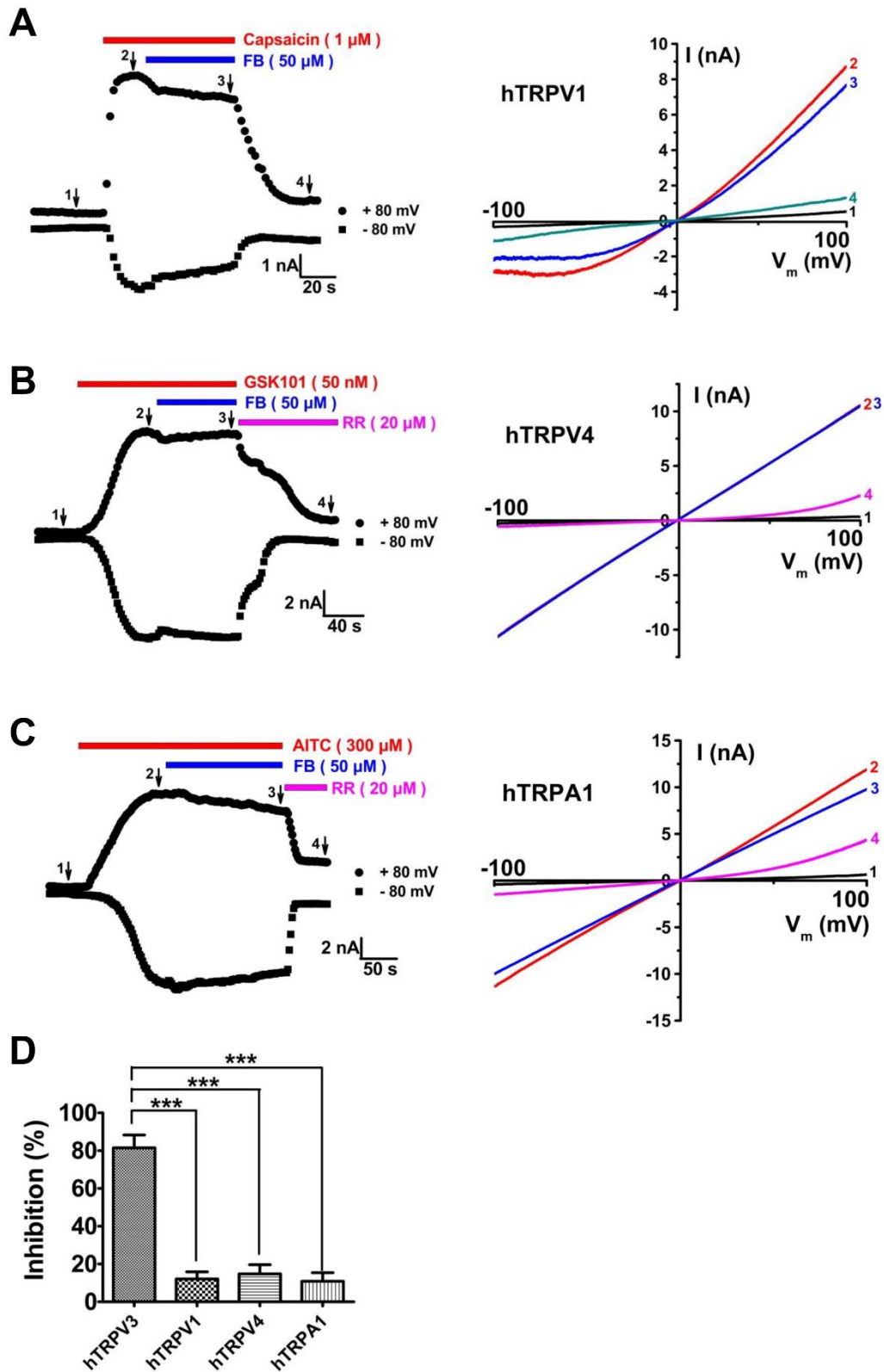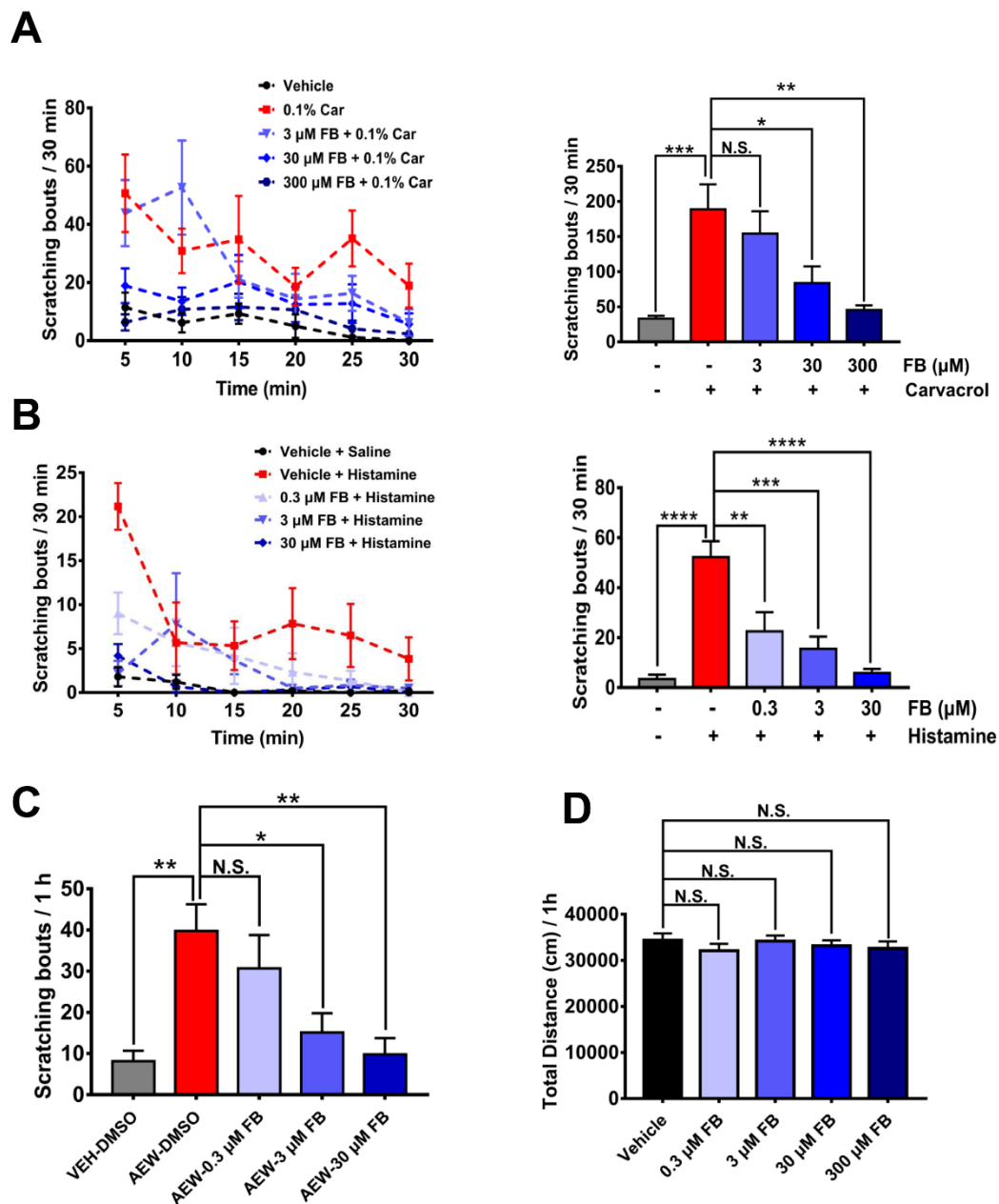
# Figure 1



## Forsythoside B
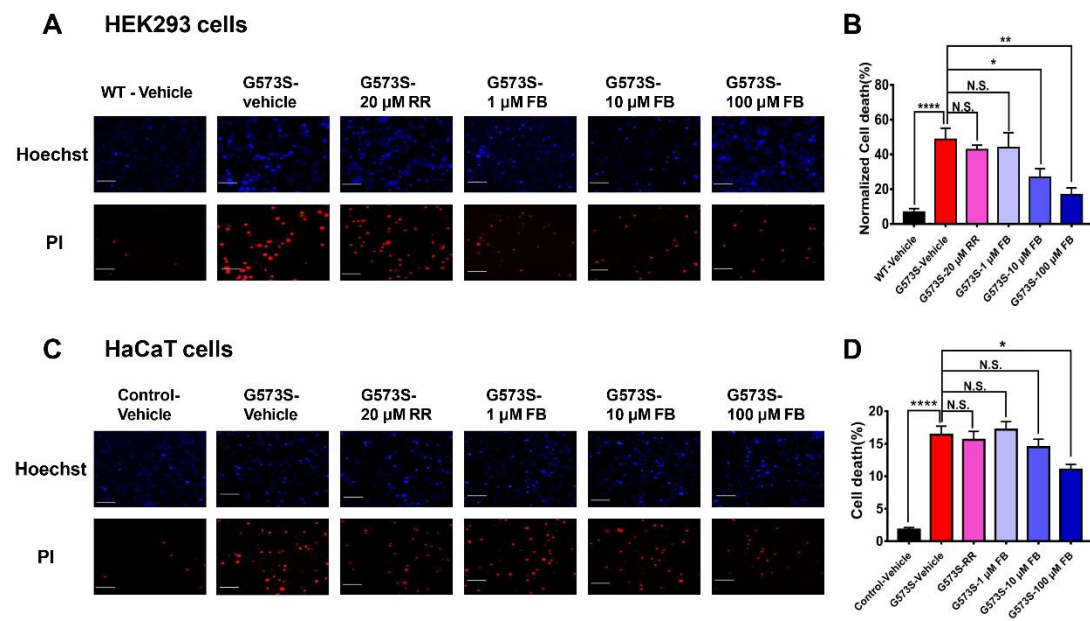
JPET # 254045
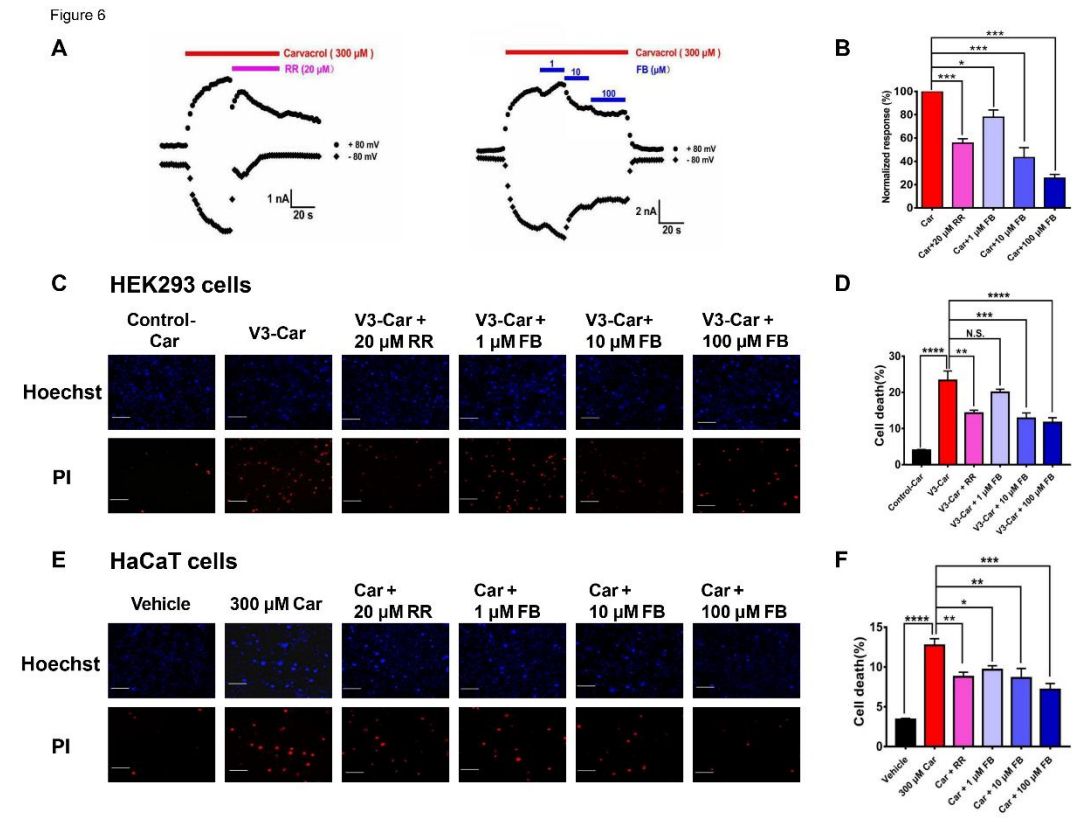
Figure 2
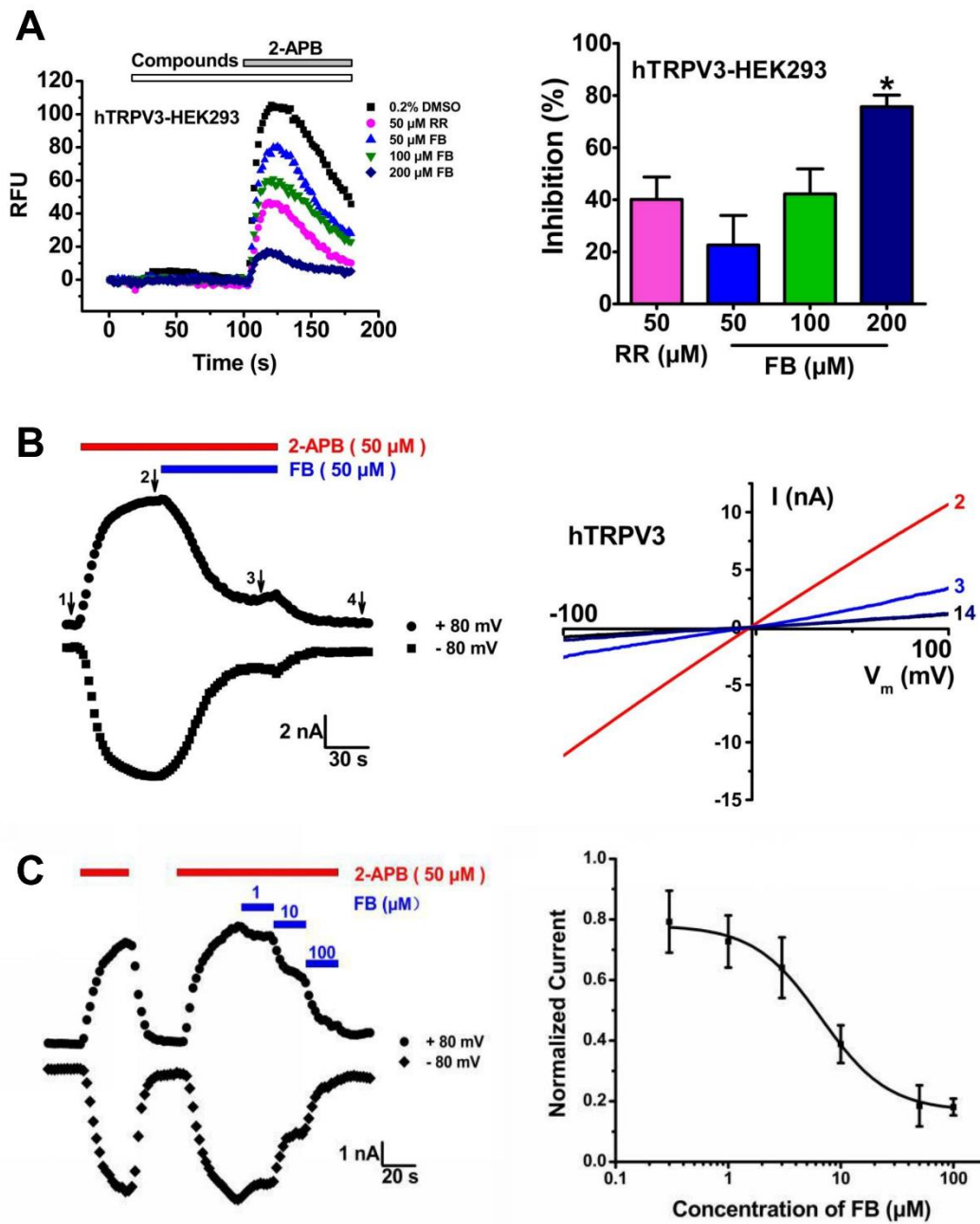
JPET # 254045

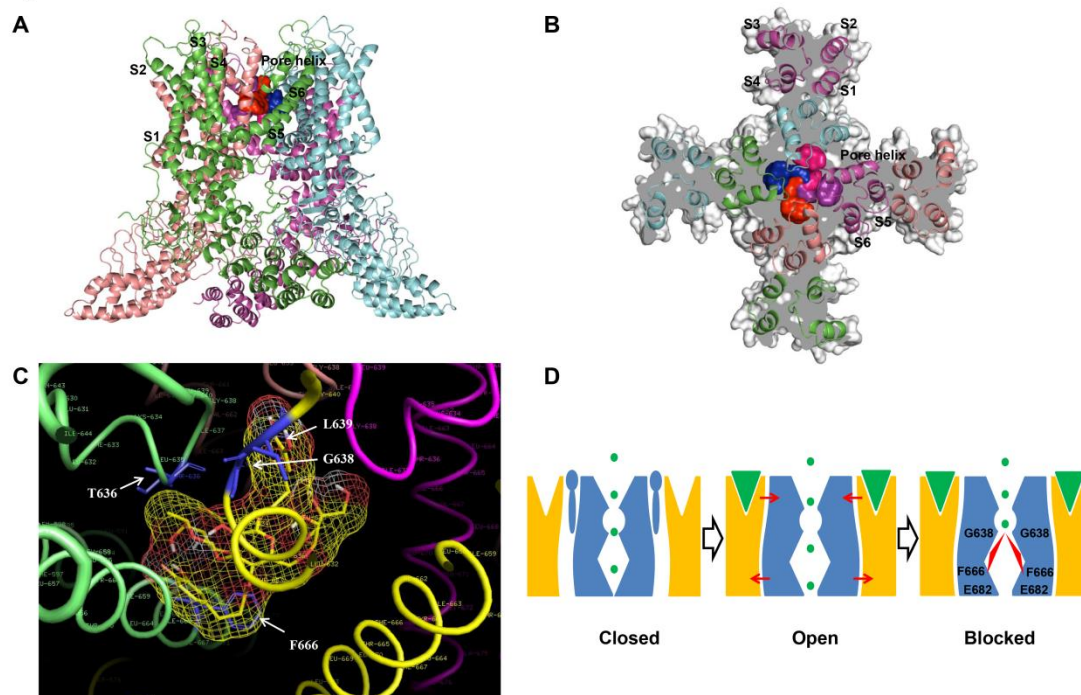Figure 3

JPET # 254045

Figure 4

JPET # 254045



Figure 5

**A**   HEK293 cells

**B**

**C**   HaCaT cells

**D**

40

JPET # 254045

Figure 6

Figure 7

Figure 8